Heliyon 9 (2023) e17838

Contents lists available at ScienceDirect

Heliyon

journal homepage: www.cell.com/heliyon

Tungsten (VI) oxide reinforced antimony glasses for radiation safety applications: A throughout investigation for determination of radiation shielding properties and transmission factors

Ghada AlMisned [a], Duygu Sen Baykal [b], Erkan Ilik [c], Mohammed Abuzaid [d], Shams A.M. Issa [e,f], G. Kilic [c], Hesham M.H. Zakaly [f,g], Antoaneta Ene [h,**,1], H.O. Tekin [d,i,*]

[a] Department of Physics, College of Science, Princess Nourah Bint Abdulrahman University, P.O. Box 84428, Riyadh, 11671, Saudi Arabia
[b] Istanbul Nisantasi University, Faculty of Engineering and Architecture, Mechatronics Engineering, 34398, Istanbul, Turkey
[c] Eskisehir Osmangazi University, Faculty of Science, Department of Physics, TR-26040, Eskisehir, Turkey
[d] Department of Medical Diagnostic Imaging, College of Health Sciences, University of Sharjah, 27272, Sharjah, United Arab Emirates
[e] Physics Department, Faculty of Science, University of Tabuk, Tabuk, 71451, Saudi Arabia
[f] Physics Department, Faculty of Science, Al-Azhar University, Assiut, 71524, Egypt
[g] Institute of Physics and Technology, Ural Federal University, Yekaterinburg, 620002, Russia
[h] Department of Chemistry, Physics and Environment, INPOLDE Research Center, Dunarea de Jos University of Galati, 47 Domneasca Street, 800008, Galati, Romania
[i] Istinye University, Faculty of Engineering and Natural Sciences, Computer Engineering Department, Istanbul, 34396, Turkey

ARTICLE INFO

Keywords:
Antimony glasses
WO_3
MCNPX
Transmission factor
Shielding

ABSTRACT

We report the functional assessment of tungsten (VI) oxide on gamma-ray attenuation properties of $60Sb_2O_3$-(40-x)$NaPO_3$-xWO_3 antimony glasses. The elemental mass-fractions and glass-densities of each glass sample are specified separately for the MCNPX Monte Carlo code. In addition to fundamental gamma absorption properties, Transmission Factors throughout a broad radioisotope energy range were measured. According to findings, holmium (Ho) incorporation into the glass structure resulted in a net increase of 0.3406 g/cm3, whereas cerium (Ce) addition resulted in a net increase of 0.2047 g/cm3. The 40% WO_3 reinforced S7 sample was found to have the greatest LAC value, even though seven glass samples exhibited identical behavior. The S2 sample had the lowest HVL values among the glass groups evaluated in this work, computed in the energy range of 0.015–15 MeV. The lowest EBF and EABF values were reported for 40% WO_3 reinforced S7 sample with the highest LAC and density values. According to the findings of this research, WO_3 will likely make a significant contribution to the gamma ray absorption properties of antimony glasses, which are employed for optical and structural modification. Therefore, it can be concluded that WO_3 may be treated monotonically and can be employed successfully in circumstances where gamma-ray absorption characteristics, optical properties, and structural qualities need to be enhanced.

* Corresponding author. Istinye University, Faculty of Engineering and Natural Sciences, Computer Engineering Department, Istanbul, 34396, Turkey.
** Corresponding author. Department of Chemistry, Physics and Environment, INPOLDE Research Center, Faculty of Sciences and Environment, Dunarea de Jos University of Galati, 47 Domneasca Street, 800008 Galati, Romania.
E-mail addresses: Antoaneta.Ene@ugal.ro (A. Ene), tekin765@gmail.com (H.O. Tekin).
[1] The author A.E. would like to thank Dunarea de Jos University of Galati, Romania, for the material and technical support.

https://doi.org/10.1016/j.heliyon.2023.e17838
Received 19 December 2022; Received in revised form 28 June 2023; Accepted 28 June 2023
Available online 30 June 2023

1. Introduction

The significance of radiation protection for patients, occupational exposure for workers, and public exposure cannot be overstated. The International Atomic Energy Agency (IAEA) is responsible for the development of fundamental radiation safety standards for nuclear power plants, medical radiation facilities, research laboratories, and accelerator centers on a global scale. The standards have been formulated based on the guidelines put forth by the International Commission for Radiological Protection (ICRP). Both individuals and organizations are required to comply with the guidelines outlined in such documents. Radiation protection may be divided into three main categories: radiation shielding, time, and distance. The level of practitioners' knowledge and awareness of the three criteria is a major factor in determining the attitude that they have toward radiation safety measures. The protective radiation shielding is made up of barriers, lead (Pb), and concrete, and it is used to provide some equipment such as personal aprons, gloves, and shields for the thyroid, eyes, and gonads. In addition, many of the medical imaging examination rooms are outfitted with transparent Pb glasses to offer patients sight. The International Atomic Energy Agency (IAEA) suggests installing separate structural radiation shielding for control consoles that also includes Pb-glass for monitoring the X-ray chamber while exposure is taking place. Traditionally, Pb and Pb-based materials have been utilized for radiation shielding procedures in many different radiation facilities. In recent years, researchers have explored the feasibility of alternative materials due to the limitations associated with Pb, including but not limited to its toxicity, low durability, and high cost. These materials are often comprised of high-density glasses [1–4], polymers [5,6], alloys [7,8], and different types of composites [9]. Glass has become a prominent candidate among the diverse range of options available for materials used in radiation shielding. The main factors can be explained based on their ease of manufacturing, lack of toxicity, strong mechanical properties, ability to resist corrosion, and a design that allows for the customization of optical and mechanical characteristics to meet the specific requirements of the intended use [10–12]. The phenomenon of natural glass formation occurs when silica-rich lava undergoes cooling, resulting in a brittle material that can be fragmented like flint, thereby generating sharp edges. In the past, the ability to create arrowheads and other rudimentary cutting tools has been facilitated through this capacity. Antimony (Sb) is a chemical element with atomic number 51 ($Z_{Sb} = 51$) found in nature as the sulfide mineral stibnite (Sb_2S_3). On the other hand, Antimony is classified as an electronegative chemical element, exhibiting a greater electronegativity than bismuth, yet a lesser electronegativity than tellurium and arsenic. The substance exhibits stability under ambient conditions, albeit it may undergo reaction with oxygen upon exposure to elevated temperatures. Antimony is utilized in the production of translucent glass, which can exhibit hues ranging from yellow to red. Antimony oxide finds application in the glass industry for the purpose of removing bubbles in optical glass, stabilizing emerald and green glass, and decolorizing specialty glasses. Compared to other antimony compounds, Sb_2S_3 exhibits greater thermal stability at elevated temperatures. Antimony-based glasses have garnered significant attention due to the substantial polarizability of Sb^{3+} ions and their diverse applications in optics and electronics. Antimony oxide-based glasses have been found to be intriguing as radiation shielding materials when compared to fluoride and tellurite glasses. This is due to their significant optical non-linearity and low phonon energy, which results in a high refractive index. [13–17]. Meanwhile, the gamma-ray absorption properties of high-density antimony oxide-doped glasses against radiation have attracted attention from researchers in recent years. In a previous study, Sayyed et al. [18] investigated the radiation shielding ability of tellurite-tungsten glasses with varying amounts of antimony oxide (Sb_2O_3). Since the comparatively lighter Sb_2O_3 translocated with the heavier WO_3 decreased the glass density, the largest Sb_2O_3 contribution caused the lowest gamma-ray absorption properties, according to their results. In another study, Zoulfakar et al., [19] analyzed the synergistic effect of Sb_2O_3 contribution for gamma-ray attenuation properties of various types of glasses. According to findings, the addition of Sb_2O_3 to those glasses increases the gamma-ray attenuation coefficients at the energies of 0.356 MeV and 0.662 MeV. Previous studies have shown that the way in which antimony oxide is translocated within the glass composition has a direct effect on the gamma-ray attenuation properties. In this study, the effects of the $NaPO_3$-WO_3 translocation as a function of the increasing WO_3 ratio in the $60Sb_2O_3$-(40-x) $NaPO_3$-xWO_3 (where x = 0–40 mol.%) glass system [20] is examined to expand on the information obtained and to advance the existing studies for antimony glasses as glass shields. The findings derived from this research have the potential to be an asset in evaluating the absorption properties of gamma rays in glass compositions that include antimony oxide additives, across various applications. The findings of this study have the potential to make a significant scientific contribution to the current knowledge of glass shields, particularly in light of the increasing utilization of glassy materials for radiation protection purposes.

2. Materials and methods

2.1. General properties of the investigated glass types and antimony oxide glasses

This study focused on investigating the radiation shielding properties of samples composed of $60Sb_2O_3$-(40-x)$NaPO_3$-xWO_3, as synthesized by Agti et al. [20]. According to their findings, the increasing density values caused by the exchange of $NaPO_3$ and WO_3 in the glass composition are candidate samples for radiation shielding investigations and applications. It has been reported that the density values increased from 4.394 g/cm^3 to 5.4 g/cm^3 by exchanging $NaPO_3$ with WO_3. It's worth mentioning that previously investigated physical, mechanical, optical, and thermal properties can be found in the reference work [20].

2.2. MCNPX simulations and computational studies for radiation shielding parameters

This study employed the MCNPX Monte Carlo simulation code and computer-supported programs to investigate the fundamental

gamma ray absorption properties of various antimony glasses doped with WO_3 [21]. The Transmission Factor (TF) is an essential parameter that can be calculated for absorbent materials, alongside other radiation shielding parameters like linear attenuation coefficients, half value layer, and mean free path. The data provided by TF entails a comparison of the photon flux values emitted by the radiation source and the photon flux that traverses the attenuator material. As a consequence of an increase in the material's absorption properties, the flux value (i.e., secondary photon flux) passing through the material decreases. This circumstance reduces the value of the secondary flux, resulting in a decline in the ratio $Flux_{secondary}/Flux_{primary}$. Consequently, the low-TF value is likewise connected with the improved absorption characteristics of the attenuator material. In this study, TF values for all glasses were examined considering several factors. Fig. 1(a) depicts the definition of a glass absorber material across a point isotropic radioactive source. Additionally, two detection areas of the same diameter are positioned in front and behind this absorber glass. The detection area closest to the source measured the primary photon flux, whereas the detection region behind the absorbing material measured the secondary photon flux. After geometrically defining the detecting regions, the F4 Tally Mesh descriptors were implemented to these zones. F4 Tally Mesh is a feature for MCNPX output that provides the average photon flux amount in a point or cell. Each simulation was performed three times, and the average results were then used. The particle count (NPS) was set at 108, and no cutting energy value was employed. Therefore, TF values dependent on energy and thickness were determined independently for each sample. On the other hand, the Phy-X/PSD [22] program is also used to compute crucial radiation shielding parameters through elemental mass fractions and densities of the investigated glasses (see Table 1). To determine the absorption properties of a material, a similar geometrical method may be used in terms of measuring the related parameters. As shown in Fig. 1(b), the quantitative relationships between the primary gamma density on the absorber material and the secondary gamma density enable the calculation of the material's attenuation coefficients. Using these obtained reduction coefficients, additional critical absorption parameters may be indirectly derived. In this work, Monte Carlo simulation outcomes and computer-assisted calculations through Phy-X/PSD were evaluated from different perspectives and a synergistic relationship was sought between them.

3. Results and discussions

3.1. Gamma-ray shielding parameters

The radiation shielding parameters of antimony oxide glasses with varying concentrations of tungsten oxide (WO_3) were examined as a function of the tungsten oxide (WO_3) ratio in the composition. Prior to the calculation phase, the densities of seven distinct glass samples S1 through S7 were shown according to the WO_3 loading ratio. As shown in Fig. 2, the S7 sample with a 40% WO_3 contribution has the highest glass density value, while the S1 sample with a minimum WO_3 contribution of 0% has the lowest density value. This clearly demonstrates the influence of $NaPO_3/WO_3$ translocation on density values, and the largest $NaPO_3$ contribution (i.e., 40%) also allowed the S1 sample to achieve the lowest density value. It is essential to understand the glass densities and the circumstances that lead to variations in density. According to the translocation ratio, the density differences between the translocation of $NaPO_3$ and WO_3 in the glass samples evaluated in this study were reflected in the glass density. In contrast to the S1 sample with 40% $NaPO_3$ and 0% WO_3 additives, the S7 sample with 0% $NaPO_3$ and 40% WO_3 additives had the highest glass density. The close relationship between the density of a substance and its gamma-ray absorption properties is the explanation for this. The linear attenuation coefficient (LAC, μ) is a parameter that is dependent on the density of a material and indicates the quantity of gamma rays that are absorbed per unit distance (cm^{-1}) [23–26]. This investigation involved the calculation of the linear attenuation coefficient (LAC) values for the studied glass samples within the energy range of 0.015–15 MeV. As depicted in Fig. 3, it is observed that the LAC values exhibit a tendency to attain their highest values within the low energy region. The prevalent process in this particular region is the photoelectric interaction, which facilitates the efficient absorption of gamma rays with low energy levels through interactions with electrons residing in the atomic orbitals of the absorbing substance. Compton Scattering predominates in the intermediate energy area, leading to a drop in LAC values

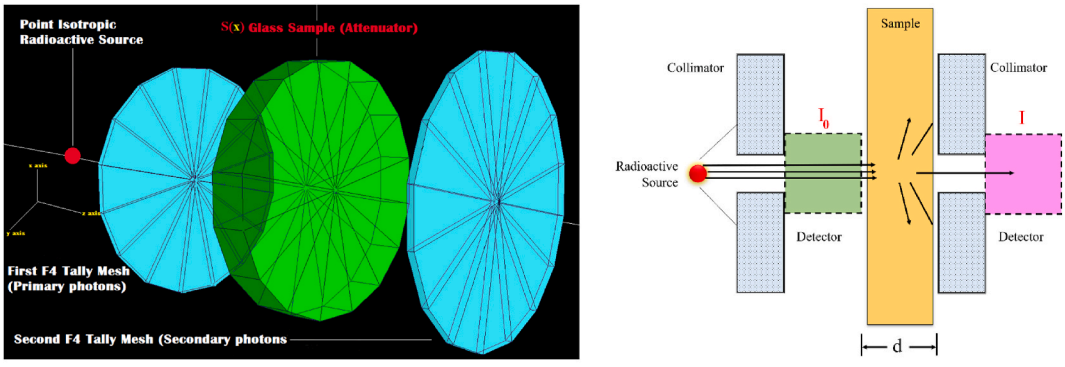

Fig. 1. (A) 3-D view of gamma-ray transmission setup obtained from MCNPX Visual Editor **(b)** A general-view of gamma-ray attenuation process through an attenuator sample.

Table 1
Sample codes, composition, elemental weight fractions and densities of the glass samples.

Sample code	O	Na	P	Sb	W	(g/cm^3) [20]
S1	0.287095	0.09019	0.121511	0.501204	0	4.394
S2	0.273909	0.078916	0.106322	0.501204	0.039649	4.613
S3	0.260722	0.067642	0.091133	0.501204	0.079298	4.729
S4	0.247536	0.056369	0.075944	0.501204	0.118946	4.87
S5	0.23435	0.045095	0.060756	0.501204	0.158595	4.99
S6	0.207978	0.022547	0.030378	0.501204	0.237893	5.17
S7	0.181606	0	0	0.501204	0.31719	5.4

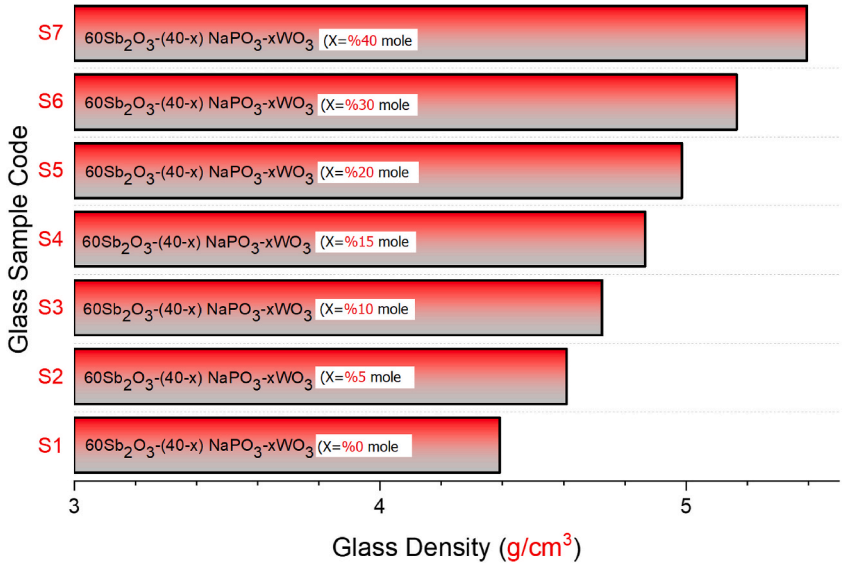

Fig. 2. Variation of glass densities for S1–S7 glass samples.

as energy increases. Photons that make primary contact with a medium would ionize orbital electrons, engage in secondary and tertiary interactions. As shown in Fig. 3, LAC values were at their lowest in the high energy area, where pair production is the predominant interaction. Similar patterns were seen in seven distinct samples throughout the three energy zones specified. However, among the samples, the S7 sample was found to have the greatest LAC values, with a maximum contribution of WO_3 and a minimum contribution of $NaPO_3$. This is due to the direct association between the LAC parameter and the material density, as well as the WO_3

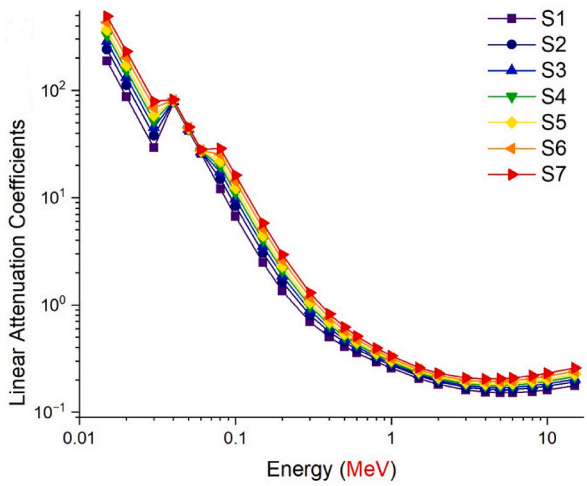

Fig. 3. Variation of linear attenuation coefficient (μ, cm^{-1}) values as a function of photon energy.

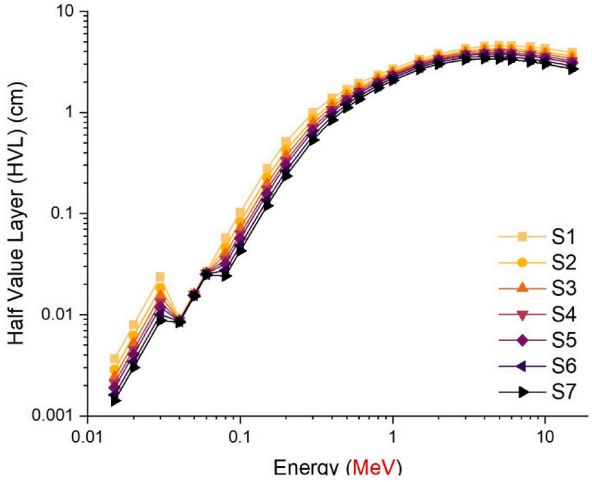

Fig. 4. Variation of half value layer (cm) values as a function of photon energy (MeV).

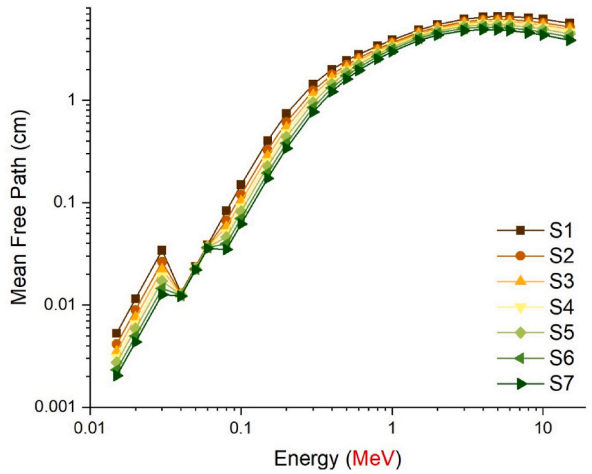

Fig. 5. Variation of mean free path (cm) values as a function of photon energy (MeV).

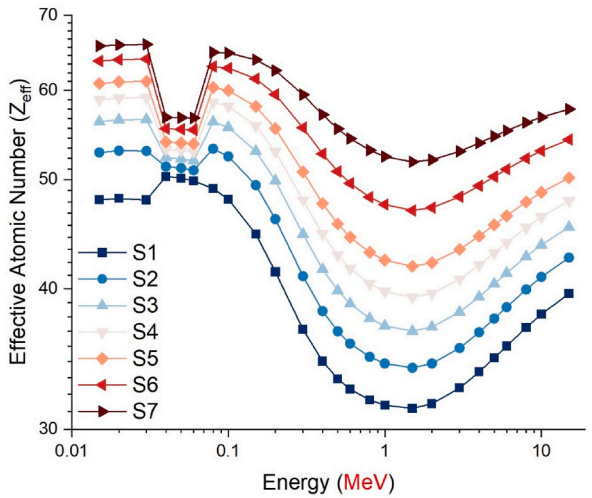

Fig. 6. Variation of effective atomic number (Z_{eff}) as a function of photon energy (MeV).

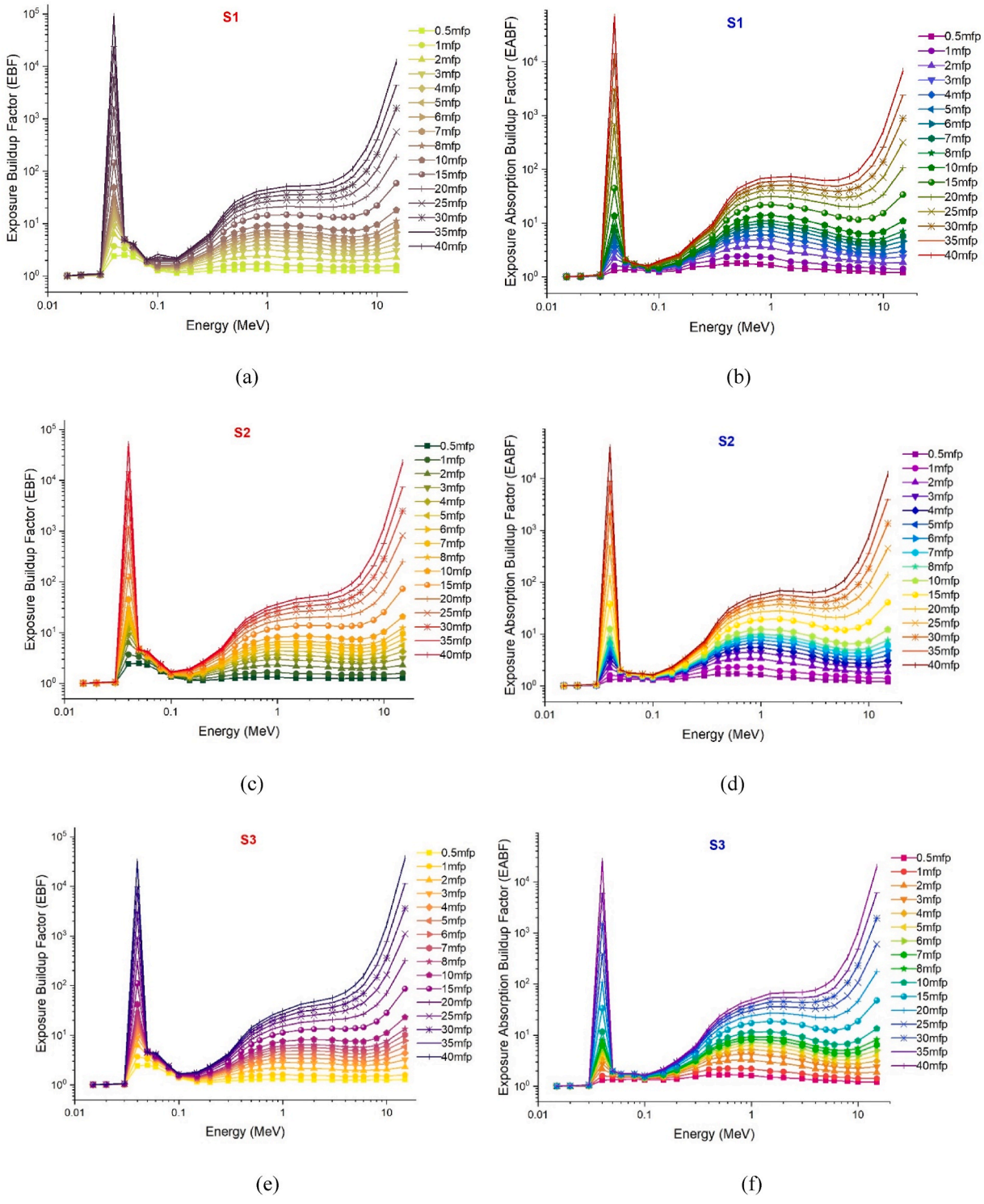

Fig. 7a. (a–f): Variation of exposure buildup factors (EBF) and energy absorption buildup factor (EABF) of investigated glasses at different mean free path values from 0.5 mfp to 40 mfp.

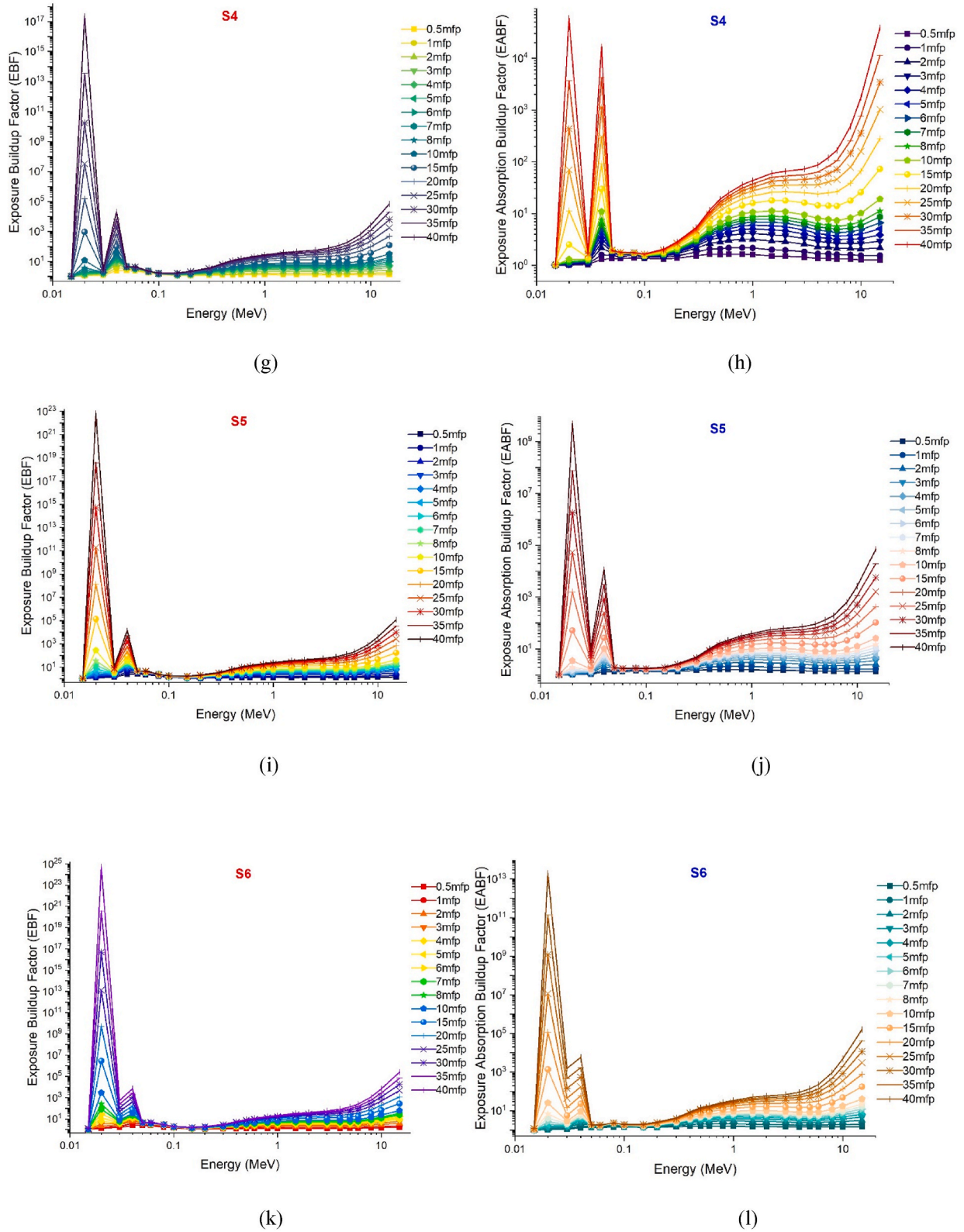

Fig. 7b. (g–l): Variation of exposure buildup factors (EBF) and energy absorption buildup factor (EABF) of investigated glasses at different mean free path values from 0.5 mfp to 40 mfp.

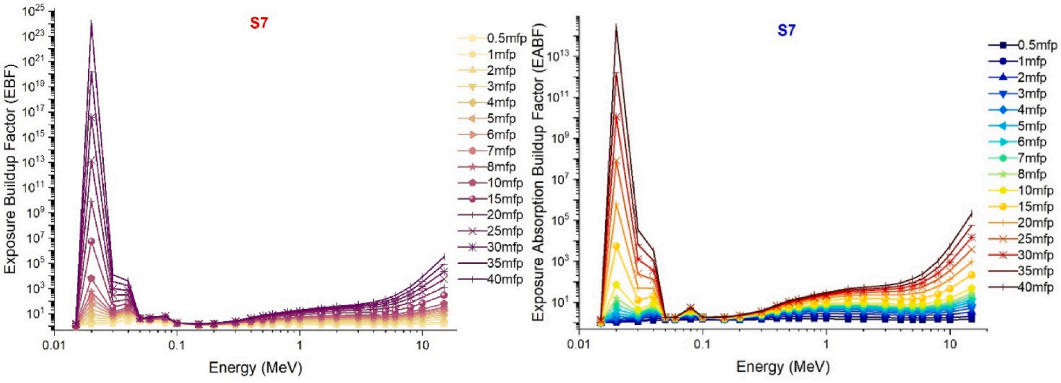

(m) (n)

Fig. 7c. (m–n): Variation of exposure buildup factors (EBF) and energy absorption buildup factor (EABF) of investigated glasses at different mean free path values from 0.5 mfp to 40 mfp.

effect, which has the higher atomic weight of the two translocated compounds in the glass structures. The half-value layer thickness (HVL), which is given in centimeters, is another metric that describes the absorption of gamma rays and specifies the minimum physical parameters that a material must meet. HVL is the thickness of a material which halves the number of gamma rays with a given energy. This value is obtained at small dimensions due to the better absorption capability of the appropriate and useful absorber materials. Observing the HVL value within minimum ranges is a significant indicator that the absorption mechanism is operating at its highest efficiency. This may be accomplished for compared materials by identifying the material with the lowest HVL value for the same energy value. In this work, the HVL values of S1–S7 glasses in the energy range of 0.015–15 MeV were determined. As shown in Fig. 4, the HVL values of all glass samples have reached their lowest values in the low energy zone and have grown according to the energy increase. This demonstrates that all seven glass samples were split by low-energy gamma rays at very thin thicknesses. This phenomenon, on the other hand, is a behavior that can be described by the weak penetrating capabilities of low-energy gammas and may be stated by the proportional rise in necessary thickness to halve the gamma-ray amount as the energy increases. The lowest HVL values for all energy values were reported for the S7 sample, which had the greatest glass density among the seven examined samples. This is interpretable by the correlation between HVL and LAC. As can be seen from Equation (1), as LAC increases, HVL decreases as a function of ln (2), providing an inverse proportion between the two variables. Therefore, the material with the highest LAC value for a given energy value will also have the lowest HVL value among the samples evaluated.

$$\mathrm{HVL} = \ln(2)/\mu \tag{1}$$

The gamma absorption parameter, which has a similar unit to HVL, is the mean free path (mfp) and is expressed in centimeters. This value represents the average route needed for consecutive interactions of gamma rays entering the medium of absorption. Like HVL, the low mfp value is indicative of the excellent gamma absorption capabilities of the material. This is because, with low mfp levels, consecutive gamma ray interactions occur at shorter distances and are exposed to a more efficient absorption process. The mfp values of the S1–S7 glass samples in the 0.015–15 MeV energy range are shown in Fig. 5. Although the mean free path (mfp) behaviors of the three distinct gamma energy areas discussed in the previous sections exhibited variation, it was observed that the S7 sample consistently displayed the lowest mfp values at each energy value. This observation suggests that the successive interactions of gamma rays within the S7 sample will take place over shorter distances compared to other glass samples, leading to a more effective absorption process in the S7 sample. Previous sections have indicated that the translocation of $NaPO_3/WO_3$ results in significant alterations in the densities of glass and, consequently, the properties of gamma ray absorption. The primary explanation for this is the largest quantity of heavier WO_3 in the S7 sample, where the $NaPO_3/WO_3$ translocation rate reaches a maximum of 40% mole. This rise in weight may be explained by the high concentration of W, which has a higher atomic number, in the S7 sample, which is also the densest glass sample. Maximal translocation optimizes the contribution of the element W ($Z_W = 74$) with a high atomic number to the gamma ray absorption process, as well as the effective atomic number value for a certain absorption energy value [27]. Fig. 6 shows the effective atomic numbers (Z_{eff}) of the examined glass samples as a function of incident gamma ray energies (MeV). Due to the biggest contribution of WO_3, the effective atomic number values of the S7 sample were the highest at every energy level. This is a significant signal that demonstrates the crucial significance that the highest WO_3 additive plays in the overall absorption process in three distinct energy regions. Meanwhile, Fig. 7a-c(a-n) displays the dependency of the exposure build-up factor (EBF) and energy absorption build-up factor (EABF) on the gamma ray energy (MeV) throughout a range of mean free path values such as 0, 5, 1, 2, 3, 4, 5, 6, 7, 8, 9, 10, 15, 20, 25, 30, 35 and 40 mfp. As the bulk of incident gamma rays are absorbed by photoelectric mechanisms, the EBF and EABF values are considerably low in the low gamma-ray energy range. Our results showed that when WO_3 was added to the investigated glass system, the EBF and EABF values reduced (i.e., from 0.5 to 40 mfp). In contrast to the high LAC and density values, the maximum-WO_3 reinforced S7 sample was found to have the lowest EBF and EABF values.

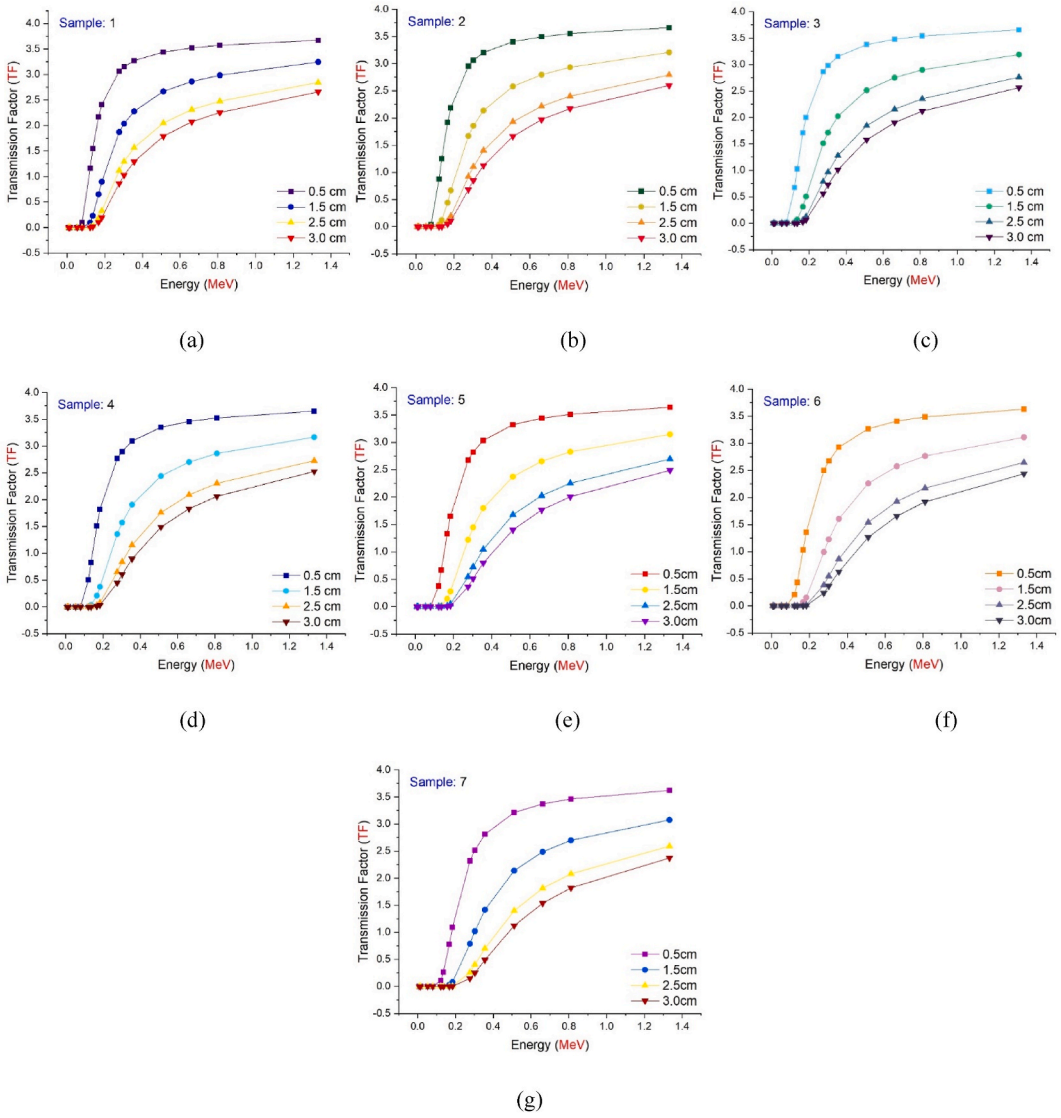

Fig. 8. (A–g): Transmission Factors (TFs) of investigated glasses as a function of used radioisotope energy (MeV) at different glass thicknesses.

Table 2
The gamma-ray energies of nuclear-type radioisotopes.

Radioisotopes	Gamma-ray energy (MeV)
^{67}Ga	0.0086, 0.0093, 0.1840
^{57}Co	0.0144, 0.1221, 0.1365
^{111}In	0.0230, 0.1710, 0.2450
^{133}Ba	0.0532, 0.0796, 0.0810, 0.2764, 0.3029, 0.3560, 0.3838
^{201}Tl	0.0710, 0.1350, 0.1670
^{99m}Tc	0.1405
^{51}Cr	0.3201
^{131}I	0.2843, 0.3645, 0.6370, 0.7229
^{58}Co	0.5110, 0.8108
^{137}Cs	0.6617
^{60}Co	1.1732, 1.3325

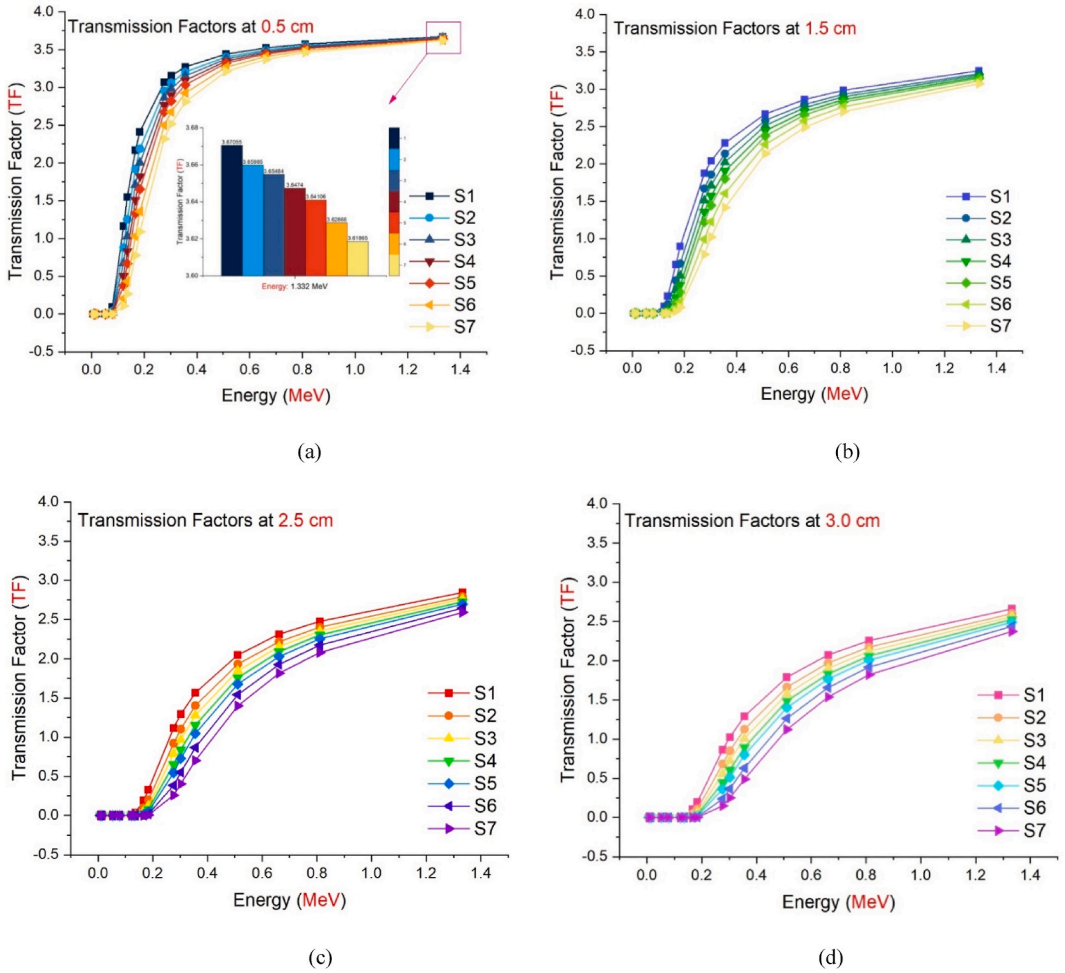

Fig. 9. Comparison of the Transmission Factors (TFs) as a function of used radioisotope energy (MeV) for different glass thicknesses.

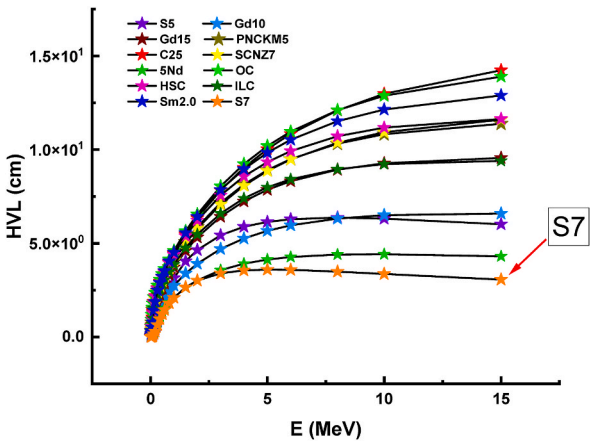

Fig. 10. Comparison of HVL values between S7 and other glass and concrete radiation shielding materials.

3.2. Transmission factors (TFs)

Fig. 8(a-g) depicts the energy dependent variance in TF values for each studied glass sample. Seven samples exhibit comparable behavioral characteristics, as seen in the figure. While TF values are lowest for low-energy radioisotopes (see Table 2), there is a considerable rise in TF values as energy increases. As indicated previously, a drop in the secondary photon flux value also results in a decrease in the TF value. For radioisotopes with low energy, the secondary photon flux seems to be minimal. Nonetheless, as seen in Fig. 8(a-g), the TF factor decreased as the glass thickness increased from 0.5 cm to 3 cm while maintaining the same energy value. This implies that gamma rays with the same energy are absorbed more as material thickness increases [28–30]. In Fig. 9(a-d), seven different glass samples with equal thicknesses were examined for their TF values and analyzed. The S7 sample showed the lowest TF values for each energy value among the four various thicknesses analyzed through TF values. This superiority of absorption over other samples, independent of thickness and energy, is an important finding regarding the maximum WO_3 contribution in the chemical configuration of S7 and hence its density. As shown in Fig. 9(a-d), the TF factor values for the energy value of 1.33 MeV in seven glass samples with a thickness of 0.5 cm are 3.67055, 3.65985, 3.65484, 3.6474, and 3.64106 for samples S1, S2, S3, S4, S5, S6, and S7, respectively., 3.62866, and 3.61865 are also presented. This clearly demonstrates the WO_3 impact even at the smallest glass thickness and greatest energy value, establishing S7 as the most effective absorber material among the investigated samples.

3.3. Benchmarking phase

In the last part of the study, the HVL values of the S7 sample, which was reported to have superior gamma-ray absorption properties, were compared with those of various conventional and new generation glass-shielding materials such as OC [28], HSC [28], ILC [28], S5 [29], Gd10 [30], Gd15 [31], PNCKM5 [32], C25 [33], SCNZ7 [34], 5Nd [35], Sm2.0 [36]. In this phase of comparison, concrete, and reinforced concrete absorbers [28] and glass shields [29–35] with various chemical configurations were tested in the energy range of 0.015–15 MeV. As a function of energy, Fig. 10 illustrates the HVL values obtained for the compared materials. In the area of low energy, the HVL values of all materials are minimal. However, it seems that the S7 sample had the lowest HVL values of all the energy gap bands examined. This is a consequence of the sample S7's intense material characteristics, which are a result of its maximum WO_3 doping and its maximum quantitative absorption properties. According to this phase of comparison, the S7 sample is a glass material that may be utilized in place of conventional and additive concrete types and can exhibit superior properties at thinner material thicknesses. The absorption superiority of the S7 sample compared to other glasses is an additional factor to consider when selecting and evaluating the most appropriate glass material. The scientific community is highly interested in investigating the radiation shielding properties of glass shields, with a focus on the impact of glass structure and various material contributions [37–44]. Hence, it is imperative to provide a more detailed account of the ideal glass configuration and reinforcement techniques to achieve optimal radiation shielding conditions. It is evident that relying solely on density as a criterion for determining the best glass option is insufficient. When faced with a decision between the S7 and other glasses that have similar optical and structural characteristics, the gamma-ray absorption capabilities of the S7 may serve as the predominant factor in determining the preferred option.

4. Conclusion

Because of significant advances in glass sciences, it is now feasible to improve the physical, mechanical, and optical qualities of the glass materials produced. Parallel to these improvements, the density of glass samples may be greatly improved by introducing various oxidized chemicals into the glass structure. The increase in density of the glasses employed in this study from 4.394 to 5.4 g/cm^3 may lessen the harmful effects of radiation. In radiation shielding procedures, the growth in density in samples where the optical band gap decreases and the refractive index of samples increases because of the addition of WO_3 is notable. The primary scientific objective of this work was to evaluate the possible impact of these preliminary findings for WO_3 on gamma-ray absorption characteristics by expanding the scope of characterization. Accordingly, several essential gamma-ray absorption parameters were determined as a function of the modified WO3 additive in seven distinct antimony glass samples utilizing advanced Monte Carlo simulation techniques and mathematical calculation techniques. The investigation yielded the following key findings.

- The S7 sample with a 40% WO_3 contribution has the highest glass density value
- The LAC values tend to reach their maximum in the low energy region.
- The S7 sample has the maximum LAC values, with a maximum contribution of WO_3 and a minimum contribution of $NaPO_3$.
- The lowest HVL values for all energy values were reported for the S7 sample, which had the maximum glass density among the seven examined samples.
- The maximal translocation optimizes the contribution of the element W ($Z_W = 74$) with a high atomic number to the gamma ray absorption process, as well as the effective atomic number value for a certain absorption energy value
- The mfp values of the S7 sample were found to be minimum at each energy value
- The EBF and EABF values reduced (i.e., from 0.5 to 40 mfp) as a function of increasing WO3 contribution in the glass compositions.
- The TF values were found to be lowest for all measured thicknesses in the glass samples assessed at low energies.
- The TF values for the maximum-WO_3 reinforced glass sample, namely S7, were the lowest for the radioisotope energies tested.

According to the findings of this research, WO_3 will likely make a significant contribution to the gamma ray absorption properties of antimony glasses, which are employed for optical and structural modification. Therefore, it is recommended to the scientific

community that WO_3 is a material that can be treated monotonically and that it is an oxide species that can be employed successfully in circumstances where gamma-ray absorption characteristics, optical properties, and structural qualities need to be enhanced. Only gamma ray absorption parameters were explored in this research. However, the findings of this research may be extended to other forms of radiation, such as neutrons and charged particles, to build a more comprehensive characterization framework. In addition, the scientific community is encouraged to explore the mechanical characteristics of these and comparable materials in future research in order to gain a full understanding of the application cases of these glasses in radiation safety operations.

Funding

Princess Nourah bint Abdulrahman University Researchers Supporting Project number (**PNURSP2023R149**), Princess Nourah bint Abdulrahman University, Riyadh, Saudi Arabia.

Author contribution statement

Ghada ALMisned: Analyzed and interpreted the data; Wrote the paper.
Duygu Sen Baykal: Erkan Ilik: Performed the experiments; Contributed reagents, materials, analysis tools or data.
Mohammed Abuzaid: Performed the experiments; Wrote the paper.
Shams A.M. Issa: Hesham M.H. Zakaly: Conceived and designed the experiments; Contributed reagents, materials, analysis tools or data.
Gokhan Kilic: Conceived and designed the experiments.
Antoaneta Ene: Analyzed and interpreted the data; Contributed reagents, materials, analysis tools or data.
Huseyin Ozan Tekin: Analyzed and interpreted the data; Contributed reagents, materials, analysis tools or data; Wrote the paper.

Data availability statement

Data will be made available on request.

Declaration of competing interest

The authors declare that they have no known competing financial interests or personal relationships that could have appeared to influence the work reported in this paper.

Acknowledgement

The authors would like to express their deepest gratitude to Princess Nourah bint Abdulrahman University Researchers Supporting Project number (**PNURSP2023R149**), Princess Nourah bint Abdulrahman University, Riyadh, Saudi Arabia.

References

[1] K. El-Egili, H. Doweidar, Y.M. Moustafa, I. Abbas, Structure and some physical properties of PbO–P2O5 glasses, Phys. B Condens. Matter 339 (4) (2003) 237–245, https://doi.org/10.1016/j.physb.2003.07.005.
[2] E. Kavaz, E. Ilik, G. Kilic, G. Almisned, H.O. Tekin, Synthesis and experimental characterization on fast neutron and gamma-ray attenuation properties of high-dense and transparent Cadmium oxide (CdO) glasses for shielding purposes, Ceram. Int. 48 (16) (2022) 23444–23451, https://doi.org/10.1016/j.ceramint.2022.04.338.
[3] L.R.P. Kassab, G.R. da Silva Mattos, S.A. Issa, G. Bilal, C.D.S. Bordon, G. Kilic, H.M.H. Zakaly, H.O. Tekin, Optical and physical behaviours of newly developed germanium-tellurium (GeTe) glasses: a comprehensive experimental and in-silico study with commercial glasses and ordinary shields, J. Mater. Sci. Mater. Electron. 32 (18) (2021) 22953–22973, https://doi.org/10.1007/s10854-021-06780-y.
[4] A.M. Vadavathi, S.K. Chinthakayala, V.S. Kollipara, G. Ramadurai, P. Gadige, Physical properties and gamma radiation shielding capability of highly dense binary bismuth borate glasses, Ceram. Int. 47 (7) (2021) 9791–9805, https://doi.org/10.1016/j.ceramint.2020.12.120.
[5] R.R. Bhosale, C.V. More, D.K. Gaikwad, P.P. Pawar, M.N. Rode, Radiation shielding and gamma ray attenuation properties of some polymers, Nucl. Technol. Radiat. Protect. 32 (3) (2017) 288–293, https://doi.org/10.2298/NTRP1703288B.
[6] A. Bhattacharya, Radiation and industrial polymers, Prog. Polym. Sci. 25 (3) (2000) 371–401, https://doi.org/10.1016/S0079-6700(00)00009-5.
[7] H.O. Tekin, O. Kilicoglu, The influence of gallium (Ga) additive on nuclear radiation shielding effectiveness of Pd/Mn binary alloys, c. https://doi.org/10.1016/j.jallcom.2019.152484, 2020.
[8] T. Singh, A. Kaur, J. Sharma, P.S. Singh, Gamma rays' shielding parameters for some Pb-Cu binary alloys, Eng. Sci. Technol. Int. J. 21 (5) (2018) 1078–1085, https://doi.org/10.1016/j.jestch.2018.06.012.
[9] N.K. Libeesh, K.A. Naseer, S. Arivazhagan, A.F. Abd El-Rehim, G. Almisned, H.O. Tekin, Characterization of Ultramafic–Alkaline–Carbonatite complex for radiation shielding competencies: an experimental and Monte Carlo study with lithological mapping, Ore Geol. Rev. 142 (2022), 104735, https://doi.org/10.1016/j.oregeorev.2022.104735.
[10] E. Ilik, Effect of heavy rare-earth element oxides on physical, optical and gamma-ray protection abilities of zinc-borate glasses, Appl. Phys. A 128 (6) (2022) 1–10, https://doi.org/10.1007/s00339-022-05642-6.
[11] N.J. AbuAlRoos, N.A.B. Amin, R. Zainon, Conventional and new lead-free radiation shielding materials for radiation protection in nuclear medicine: a review, Radiat. Phys. Chem. 165 (2019), 108439, https://doi.org/10.1016/j.radphyschem.2019.108439.
[12] V.P. Singh, N.M. Badiger, J. Kaewkhao, Radiation shielding competence of silicate and borate heavy metal oxide glasses: comparative study, J. Non-Cryst. Solids 404 (2014) 167–173, https://doi.org/10.1016/j.jnoncrysol.2014.08.003.
[13] K. Ouannes, M.T. Soltani, M. Poulain, G. Boulon, G. Alombert-Goget, Y. Guyot, A. Pillonnet, K. Lebbou, Spectroscopic properties of Er3+-doped antimony oxide glass, J. Alloys Compd. 603 (2014) 132–135, https://doi.org/10.1016/j.jallcom.2014.02.008.

[14] A.E. Ersundu, M. Çelikbilek, M. Baazouzi, M.T. Soltani, J. Troles, S. Aydin, Characterization of new Sb2O3-based multicomponent heavy metal oxide glasses, J. Alloys Compd. 615 (2014) 712–718, https://doi.org/10.1016/j.jallcom.2014.07.024.

[15] A.M. Zoulfakar, A.M. Abdel-Ghany, T.Z. Abou-Elnasr, A. G, S.M. Mostafa Salem, H.H. El-Bahnaswy, Effect of antimony-oxide on the shielding properties of some sodium-boro-silicate glasses, Appl. Radiat. Isot. 127 (April) (2017) 269–274, https://doi.org/10.1016/j.apradiso.2017.05.007.

[16] S.Y. Marzouk, F.H. Elbatal, Infrared and UV-visible spectroscopic studies of gamma-irradiated Sb 2O3-B2O3 glasses, J. Mol. Struct. 1063 (1) (2014), https://doi.org/10.1016/j.molstruc.2014.01.081, 328–35.

[17] H.O. Tekin, G. Susoy, S.A.M. Issa, A. Ene, G. Almisned, Y.S. Rammah, F.T. Ali, M. Algethami, H.M.H. Zakaly, Heavy metal oxide (HMO) glasses as an effective member of glass shield family: a comprehensive characterization on gamma ray shielding properties of various structures, J. Mater. Res. Technol. 18 (2022) 231–244, https://doi.org/10.1016/j.jmrt.2022.02.074.

[18] M.I. Sayyed, H.O. Tekin, E.E. Altunsoy, S.S. Obaid, M. Almatari, Radiation shielding study of tellurite tungsten glasses with different antimony oxide as transparent shielding materials using MCNPX code, J. Non-Cryst. Solids 498 (2018) 167–172, https://doi.org/10.1016/j.jnoncrysol.2018.06.022.

[19] A.M. Zoulfakar, A.M. Abdel-Ghany, T.Z. Abou-Elnasr, A.G. Mostafa, S.M. Salem, H.H. El-Bahnaswy, Effect of antimony-oxide on the shielding properties of some sodium-boro-silicate glasses, Appl. Radiat. Isot. 127 (2017) 269–274, https://doi.org/10.1016/j.apradiso.2017.05.007.

[20] F.Z. Agti, M.T. Soltani, L.F. Santos, A. Messaoudi, N. Guesmia, D.D. Ligny, Physical, mechanical properties and optical dispersion in Sb2O3-NaPO3-WO3 glasses, J. Non-Cryst. Solids 576 (2022), 121249, https://doi.org/10.1016/j.jnoncrysol.2021.121249.

[21] RSICC Computer Code Collection, MCNPX User's Manual Version 2.4.0. MonteCarlo N-Particle Transport Code System for Multiple and High Energy Applications, 2002.

[22] E. Şakar, Ö.F. Özpolat, B. Alım, M.I. Sayyed, M. Kurudirek, Phy-X/PSD: development of a user friendly online software for calculation of parameters relevant to radiation shielding and dosimetry, Radiat. Phys. Chem. 166 (2020), 108496, https://doi.org/10.1016/j.radphyschem.2019.108496.

[23] B. Oruncak, Gamma-ray shielding properties of Nd2O3 added iron-boron-phosphate based composites, Open Chem. 20 (1) (2022) 237–243, https://doi.org/10.1515/chem-2022-0143.

[24] F. Waheed, M. İmamoğlu, N. Karpuz, H. Ovalıoğlu, Simulation of neutrons shielding properties for some medical materials, Int. J. Comput. Exp. Sci. Eng. 8 (1) (2022) 5–8, https://doi.org/10.22399/ijcesen.1032359.

[25] R. Boodaghi Malidarre, İ. Akkurt, K. Gunoglu, H. Akyıldırım, Fast neutrons shielding properties for HAP-Fe2O3 composite materials, Int. J. Comput. Exp. Sci. Eng. 7 (3) (2021) 143–145, https://doi.org/10.22399/ijcesen.1012039.

[26] D. Şen Baykal, H. Tekin, R. Çakırlı Mutlu, An investigation on radiation shielding properties of borosilicate glass systems, Int. J. Comput. Exp. Sci. Eng. 7 (2) (2021) 99–108, https://doi.org/10.22399/ijcesen.960151.

[27] I. Akkurt, Effective atomic numbers for Fe–Mn alloy using transmission experiment, Chin. Phys. Lett. 24 (2007) 2812, https://doi.org/10.1088/0256-307X/24/10/027.

[28] I.I. Bashter, Calculation of radiation attenuation coefficients for shielding concretes, Ann. Nucl. Energy 24 (1997) 1389–1401, https://doi.org/10.1016/S0306-4549(97)00003-0.

[29] G. Almisned, W. Elshami, S.A.M. Issa, G. Susoy, H.M.H. Zakaly, M. Algethami, Y.S. Rammah, A. Ene, S.A. Al-Ghamdi, A.A. Ibraheem, H.O. Tekin, Enhancement of gamma-ray shielding properties in cobalt-doped heavy metal borate glasses: the role of lanthanum oxide reinforcement, Materials 14 (2021) 7703, https://doi.org/10.3390/ma14247703.

[30] Y. Al-Hadeethi, M.I. Sayyed, B.M. Raffah, E. Bekyarova, Y.S. Rammah, Optical properties and radiation shielding features of Er3+ ions doped B2O3–SiO2–Gd2O3–CaO glasses, Ceram. Int. 47 (2021) 3421–3429, https://doi.org/10.1016/j.ceramint.2020.09.187.

[31] F. Zaman, G. Rooh, N. Srisittipokakun, H.J. Kim, E. Kaewnuam, P. Meejitpaisan, J. Kaewkhao, Scintillation and luminescence characteristics of Ce3+doped in Li2O–Gd2O3–BaO–B2O3 scintillating glasses, Radiat. Phys. Chem. 130 (2017) 158–163, https://doi.org/10.1016/j.radphyschem.2016.08.016.

[32] A. Alalawi, M.S. Al-Buriahi, Y.S. Rammah, Radiation shielding properties of PNCKM bioactive glasses at nuclear medicine energies, Ceram. Int. 46 (2020) 15027–15033, https://doi.org/10.1016/j.ceramint.2020.03.033.

[33] G. Susoy, E.E.A. Guclu, O. Kilicoglu, M. Kamislioglu, M.S. Al-Buriahi, M.M. Abuzaid, H.O. Tekin, The impact of Cr2O3 additive on nuclear radiation shielding properties of LiF–SrO–B2O3 glass system, Mater. Chem. Phys. 242 (2020), 122481, https://doi.org/10.1016/j.matchemphys.2019.122481.

[34] H. Akyildirim, E. Kavaz, F.I. El-Agawany, E. Yousef, Y.S. Rammah, Radiation shielding features of zirconolite silicate glasses using XCOM and FLUKA simulation code, J. Non-Cryst. Solids 545 (2020), 120245, https://doi.org/10.1016/j.jnoncrysol.2020.120245.

[35] H.M.H. Zakaly, H.O. Tekin, S.A.M. Issa, A.M.A. Henaish, E.M. Ahmed, Y.S. Rammah, Fabrication, physical, structure characteristics, neutron and radiation shielding capacity of high-density neodymio-cadmium lead-borate glasses: Nd2O3/CdO/PbO/B2O3/Na2O, Appl. Phys. Mater. Sci. Process 128 (2022), https://doi.org/10.1007/s00339-022-05689-5, 1–17.

[36] H.M.H. Zakaly, Y.S. Rammah, H.O. Tekin, A. Ene, A. Badawi, S.A.M. Issa, Nuclear shielding performances of borate/sodium/potassium glasses doped with Sm3 + ions, J. Mater. Res. Technol. 18 (2022) 1424–1435, https://doi.org/10.1016/j.jmrt.2022.03.030.

[37] A.A. Menazea, A.M. Abdelghany, N.A. Hakeem, W.H. Osman, F.H. Abd El-kader, Precipitation of silver nanoparticles in borate glasses by 1064 nm Nd: YAG nanosecond laser pulses: characterization and dielectric studies, J. Electron. Mater. 49 (2020) 826–832.

[38] E.M.A. Khalil, F.H. El-Batal, Y.M. Hamdy, H.M. Zidan, M.S. Aziz, A.M. Abdelghany, UV-visible and IR spectroscopic studies of gamma irradiated transition metal doped lead silicate glasses, Silicon 2 (2020) 49–60.

[39] I.S. Elashmawi, A.M. Abdelghany, N.A. Hakeem, Quantum confinement effect of CdS nanoparticles dispersed within PVP/PVA nanocomposites, J. Mater. Sci. Mater. Electron. 24 (2013) 2956–2961.

[40] F.H. ElBatal, A.M. Abdelghany, H.A. ElBatal, Characterization by combined optical and FT infrared spectra of 3d-transition metal ions doped-bismuth silicate glasses and effects of gamma irradiation, Spectrochim. Acta Mol. Biomol. Spectrosc. 122 (2014) 461–468.

[41] A.M. Abdelghany, Y.S. Rammah, Transparent alumino lithium borate glass-ceramics: synthesis, structure and gamma-ray shielding attitude, J. Inorg. Organomet. Polym. Mater. 31 (2021) 2560–2568.

[42] Norah A.M. Alsaif, I.O. Olarinoye, Y.S. Rammah, The role of titania on gamma and neutron attenuation competence of sodium lead borosilicate glasses, J. Australas. Ceram. Soc. 58 (2022) 939–947.

[43] Norah A.M. Alsaif, A.M. Abdelghany, Y.S. Rammah, I.O. Olarinoye, N.V. Kudrevatykh, A.S. Abouhaswa, A comprehensive study on optical features, gamma photon buildup factors and neutron shielding capability of B2O3-SB2O3-Li2O-Bi2O3 glasses, Bull. Chem. Soc. Ethiop. 36 (4) (2022) 949–962.

[44] A.M. Abdelghany, Norah A.M. Alsaif, M.A. Madshal, H.A. ElBatal, Y.S. Rammah, W. Awad, Structural, optical and radiation shielding parameters of sodium aluminium borate glasses modified with chromium oxide, Radiat. Phys. Chem. 207 (2023), 110861.